Simultaneous Characterization of Optical and Rheological properties of Carotid Arteries via Bimodal Spectroscopy: Experimental and Simulation Results

E. Pery*, W.C.P.M. Blondel*, J. Didelon, A. Leroux, and F. Guillemin

Abstract—The present study aimed at identifying potential correlations between rheological and optical properties of artery rings before and after cryopreservation, at different deformations, using experimental and simulation results. For experiments, an artery ring uniaxial mechanical test bench was coupled to fibered optical spectroscopes measuring 410 nm-excited autofluorescence and 650-850 nm elastically back-scattered intensity spectra. Furthermore, we developed a statistical simulation program of light transport and fluorescence adapted to our specific experimental configuration. Both spectroscopies gave intensity spectra with higher amplitude for the cryopreserved samples. These observations are to be related to histological modifications affecting the arterial wall of post-cryopreserved samples. We also observed significative spectral amplitude variations (increasing autofluorescence intensity and decreasing diffuse reflectance) as a function of the circumferential strains (0-60%).Using the simulation, we identified values of absorption, diffusion and anisotropy coefficients and their variations as a function of state (fresh-cryopreserved), strains (0, 30%, 60%) and wavelengths (700, 740, 780 nm). The media and the adventice are respectively less and more absorbing for post-cryopreserved rings and it is the opposite for the fresh ones at higher wavelengths. Absorption and diffusion coefficients are slightly higher, whatever the wavelengths and strains, for the fresh than for the cryopreserved samples.

Index Terms—autofluorescence, elastic scattering, optical parameters, biomechanics, artery.

I. INTRODUCTION

FIBERED optical methods of diagnosis such as autofluorescence and diffuse reflectance spectroscopies are used to characterize biological tissues non invasively and non destructively [1]. The principle consists in lighting a living tissue with an incident light flux which is then absorbed, elastically scattered or gives rise to intrinsic fluorescence. Consequently, the spectral characteristics of the outcoming light intensity measured either in transmission or in reflectance configurations can be related to the morphological, anatomical characteristics and biochemical or metabolic activity of the tissue, which vary with aging or diseases. Furthermore, the differentiation degree between various types or pathological stages of biological tissues (healthy, inflammatory, cancerous, atheromatous,...) can be increased through the complementarity of autofluorescence and light scattered spectra collected in bimodal reflectance spectroscopy [2] [3].

The fact that fresh and cryopreserved arterial segments are characterized by differences in terms of cellular viability [4] [5] and structure [6] result in modifications of the bio-optical responses of the vascular tissue [7] [8] (absorption, diffusion, fluorescence). Thus, by identifying some correlation existing between the optical properties of arterial tissues and their state or level of mechanical constraints or strains, new *in vitro* and *in vivo* contactless and atraumatic methods of characterization of these mechanical properties can be considered. Among the various types of *in vivo* and *in vitro* systems (uniaxial, biaxial...) developed to study the bio-mechanical behavior of vascular tissues [7] [9] [10], *in vitro* tests on rings or segments are classical and simple to implement. They provide the acquisition of complete data under "controlled" environment.

The aim of our work was to study the variations of optical properties (absorption, scattering, and fluorescence) of fresh and post-cryopreserved artery rings (pig common carotid) with reference to mechanical strains applied to them (under uniaxial elongation). Preliminary results already published by our group have confirmed the existence of differences between arteries before and after cryopreservation, in their rheological behaviour [4] [11] and in their optical (spectral) behaviour using fluorescence spectroscopy [11] or elastic scattering spectroscopy [12]. This paper presents final and original results of our works concerning first the characterization of different biomechanical states of these artery rings (fresh / post-cryopreserved, various circumferential deformations) using diffuse reflectance and autofluorescence spectral data, and second the variations of the absorption ("pure" absorption and absorption for fluorescence), scattering and anisotropy coefficients of the artery wall with its mechanical deformation using Monte Carlo simulation of steady-state light transport

E. Pery* and W.C.P.M. Blondel* are with the Health Engineering Group in the Automatic Control Research Center in Nancy-University (UMR 7039 CRAN CNRS-UHP-INPL), 2 avenue de la Forêt de Haye F-54516 Vandoeuvre-les-Nancy, France. (e-mails of the corresponding authors: emilie.pery@ensem.inpl-nancy.fr, walter.blondel@ensem.inpl-nancy.fr).

J. Didelon is with the Laboratory of Automated Medical Instrumentation in Cancerology (IMAC)in the anti-cancer center"Centre Alexis Vautrin", 54511 Vandoeuvre-les-Nancy, France (e-mail: j.didelon@nancy.fnclcc.fr).

A. Leroux is with the Anatomopathologic Department in the "Centre Alexis Vautrin", 54511 Vandoeuvre-les-Nancy, France (e-mail: a.leroux@nancy.fnclcc.fr).

F. Guillemin is a surgeon and director in the "Centre Alexis Vautrin", 54511 Vandoeuvre-les-Nancy, France (e-mail: f.guillemin@nancy.fnclcc.fr).

Fig. 1. Schematic representation of the experimental set-up configuration. x is the length applied to elongate the vascular ring in the direction of $\vec{F}$, the force measured. Monochromatic (LASER) and wide wavelength band (LED) light excitations are consecutively injected throughout the excitation fiber. The backscattered intensity spectra are measured from the two collecting fibers corresponding to two distances between excitation and emission fibers at distal tip of the probe (0.53 and 1.74 mm).

and fluorescence within a multi-layer model over the wavelength band [470-850 nm].

II. MATERIALS AND METHODS

A. Experimental system and calibrations

The experimental set-up is based on an apparatus already described in detail in [11] [12]. Briefly, it consists of a mechanical test bench to which two fibered spectroscopic measurement systems were added (Fig. 1): an AutoFluorescence Spectroscope (AFS), which provides the autofluorescence intensity spectra of tissues excited at 410 nm ± 10 nm FWHM (Full Width at Half Maximum) and an Elastic Scattering Spectroscope (ESS), which can record diffuse reflectance spectra in the visible-to-NIR (Near InfraRed) wavelength band. The multiple fiber optic probe configuration enable the acquisition of backscattered intensity spectra from two collecting fibers corresponding to two distances between excitation (illumination) and emission (collecting) fibers at distal end of the probe (0.53 mm and 1.74 mm, called respectively channel 1 and channel 2) [13] [14] [15].
Step-by-step elongation was performed by micrometric displacements (resolution: 0.02 mm) applied in the direction of the circumferential traction strength measured $\overrightarrow{F}$ as sketched in Fig. 1. Before starting an experiment, the system was calibrated in force using an extension stainless steel spring (average diameter: 5.5 mm, wire section: 0.5 mm and 78.25 reels). The fibered spectrofluorimeter calibration required a light power adjustment using a power meter (841PE, power sensor UV 818-UV, Newport). To account for the wavelength dependence of the light source, the fiber spectral transmission and the spectrometer response, a reference measurement of reflectance from a spectrally flat reflectance standard (spectralon®) was regularly performed [1]. Optical resolution of the acquisition system was 8 nm. The calibration procedure was reiterated for each new sample.

B. Biological materials and protocol of tests

Segments of common carotid arteries were post-mortem surgically dissected from four young pigs (20 to 30 kg, 4 to 6 months old). All animals received human care in compliance with the European legislation for animal care. These segments were temporarily stored at 4C in culture medium M199 supplemented with antibiotics (penicillin, streptomycin) and fungicide (fungizone) until in vitro tests started.

Overall, four pig carotid arteries of about 40-50 mm uniform length were exploited and cut in thirty two rings of about 4 mm length. Half of rings of each fresh artery segment were systematically tested within two days following surgery. The other half of fresh, not-tested artery, were directly cryopreserved for one month. The freezing medium was copied from the protocol of tissue banks [5] and cryopreservation was performed following a classical step-by-step temperature descent protocol down to -150C in nitrogenize liquid.

The in vivo length, external diameter and thickness of each segment of artery were systematically measured before testing, as described in [11]. Each ring has a 4 mm length so as to provide an appropriate contact area with the fiber probe (2 mm diameter). Before mechanical tests began, each sample was pre-conditioned to an elongation of 10% initial length during five minutes on the test bench. At each elongation step applied to an arterial ring under test conditions, the sample was able to relax for constraints during one minute before proceeding to the force measurement. Circumferential strains ($\varepsilon_{\theta\theta}$) were applied to the samples from 0% to 60% by steps of 10%, from reference unloaded state. Corresponding forces $\overrightarrow{F}$ are measured for stress calculations.

C. Mechanical model and parameter calculation

The tested rings were considered as uniform, circular, cylindrical and incompressible thin-walled short tubes. The carotid artery wall was also assumed to behave as an anisotropic, orthotropic, non-linear elastic continuum and homogeneous material. A theory of large elastic deformations was used [16] [17]. Considering a model of annular sample under uniaxial traction [18], circumferential stress $\sigma_{\theta\theta}$ (N/m^2) and strain $\varepsilon_{\theta\theta}$ can be given by relations (1).

$$\sigma_{\theta\theta} = \frac{F}{2.L.h} \approx \frac{F.x}{V} \quad \text{and} \quad \varepsilon_{\theta\theta} = \ln\left(\frac{x}{x_0}\right) \qquad (1)$$

where x_0 and x (mm) are the transverse lengths of the ring in the initial state and under imposed strain respectively, F is the measured traction strength (N) and $V \cong 2.L.h.x$ is the total arterial ring volume, with L and h (mm) respectively the axial length and the thickness of the artery wall of the annular sample under test. Arterial ring ends in contact of the gripping hooks are not considered in stress calculation because they undergo additional local stresses [19].
As the ratio of stress to strain is nonlinear, the incremental elastic modulus E_{inc}, given by (2), was also determined [6].

$$E_{inc} = \frac{\Delta\sigma_{\theta\theta}}{\Delta\varepsilon_{\theta\theta}} \qquad (2)$$
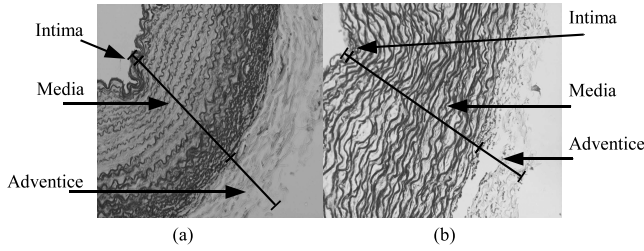
Fig. 2. Images of histological slices of (a) fresh and (b) cryopreserved artery rings (transmission microscopy, Growth X10).

D. Spectroscopic data pre-processing

Three data processing steps were applied to raw autofluorescence and back-scattered light spectra. For every measurement (at each elongation), five raw spectra were automatically acquired at the same point for both autofluorescence and diffuse reflectance and averaged in order to improve the signal to noise ratio.

Then, a polynomial smoothing filter (Savitzky-Golay algorithm) [20] [21] was applied to the autofluorescence spectra to further reduce high frequency noises. For autofluorescence, a standardization was required for proper shape comparison between the various spectral curves [22]. We choose a standard normalization with reference to the area under the curve, which, in our case, reduces the area under the curve between 470 and 810 nm to unity such as:

$$I_{norm}(\lambda_i) = I(\lambda_i)/b \quad \text{with} \quad b = \Delta\lambda \sum_{i=1}^{N} I(\lambda_i) \quad (3)$$

where $I(\lambda_i)$ and $I_{norm}(\lambda_i)$ denote respectively the measured and normalized autofluorescence light intensities at wavelength λ_i, N is the total number of curve points (number of sampled wavelength values) and $\Delta\lambda$ is the fixed wavelength's sampling step (0.5 nm).

For elastic scattering measurements, spectral response correction and amplitude standardization are intrinsically taken into account in the diffuse reflectance calculation defined as [1]:

$$R(\lambda) = \frac{S_{tissue}(\lambda) - S_{tissue\ background}(\lambda)}{S_{ref}(\lambda) - S_{ref\ background}(\lambda)} \quad (4)$$

where S_{tissue}, $S_{tissue\ background}$, S_{ref} and $S_{ref\ background}$ correspond to mean filtered spectra measured respectively on tissue with light excitation switched on and off (background measure including ambient light and detector dark current) and on spectralon® reference (spectrally flat response) with light excitation switched on and off.

E. Histological analysis

Fig. 2 shows an exemple of typical transverse histological cuts of fresh and cryopreserved artery rings, imaged using a transmission microscope. A Weigert staining was carried out to reveal collagen and elastin fibers.

In the unloaded fresh sample, the media's fibrous network looks continuous with sinuous fibers. Indeed, on the image of the unloaded cryopreserved sample, the fibrous network seem more slackened and less folded up, showing an extracellular matrix looser and less dense than in the fresh sample. These data are in agreement with histological results of studies already published on cryopreserved arteries [23]. We observe a radial distribution of fiber network, which is less homogeneous for the fresh rings (highest density outwards from the media) than for the cryopreserved ones (radial distribution homogeneous in the media).

These purely morpho-histological observations already let us predict of possible differences in optical behavior between fresh and post-cryopreserved samples.

F. Optical model, parameters and numerical simulation

We developed a simulation program (Monte Carlo) of spatially resolved steady-state light transport (absorption and multiple diffusion) based on MCML code [24] and from [25] adapted to our specific experimental configuration (described in [26]), to which multiple fluorescence was added. Briefly, we used a three-layer model of artery wall (adventice, media and intima), each layer being described by thickness, absorption coefficient $\mu_a(\lambda)$, scattering coefficient $\mu_s(\lambda)$, refractive index n, and optical anisotropy factor $g(\lambda)$. g is defined as the mean cosine of the rediffusion angle in the optical phase function. The Henyey-Greenstein phase function expression was implemented in our simulation program. With help of the initial mean thickness and total volume of each artery ring measured before spectroscopic tests start (see section II-B), we calculated the total thickness h_t of the wall at each different circumferential strain applied, considering the incompressibility of the samples at these strains i.e. constant volume (see section II-C). These different thickness values varying with circumferential strains were used in our simulation model. In this three-layered model, we considered that the thickness of each layer was a constant proportion of the total thickness (whatever the strain). Based on histological observations, we choose 45%, 50% and 5% of h_t for the adventice, the media and the intima respectively.

As we previously noticed in [26], the simulated elastic scattering spectra are not properly correlated with experimental results if we use the few values of optical coefficients for arteries available in the literature [27] [28]. Therefore, we calculated optimized values for the optical parameters $\mu_a^A(\lambda)$, $\mu_a^M(\lambda)$, $\mu_a^I(\lambda)$, $\mu_s^A(\lambda)$, $\mu_s^M(\lambda)$, $\mu_s^I(\lambda)$ and $g^A(\lambda)$, $g^M(\lambda)$ and $g^I(\lambda)$ of the three layers Adventice (A), Media (M), and Intima (I).

We decided to keep the numerical values of $n(\lambda)$ constant for all layers as found in the literature [27] [28]. The simulation was performed wavelength-by-wavelength by increasing values from 470 to 850 nm with a wavelength step of 10 nm. All simulated spectra and optical parameters were then defined as vectors of $N = 21$ values. We then searched values of the optical parameters for every wavelength between 470 and 850 nm (10 nm step), which minimize the cost function hereafter (equation 5).
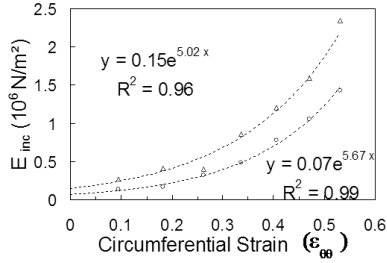
Fig. 3. Mean Incremental Elastic Modulus E_{inc} as a function of circumferential strain $\varepsilon_{\theta\theta}$ for fresh (circles) and cryopreserved samples (triangles) (significant difference between fresh and cryopreserved sample curves: $p < 0.05$). Dotted curves represent the exponential approximations of both experimental data sets, with R^2 their respective coefficient of determination.

$$Error(p) = \sum_{i=1}^{N} |y_{exp}(\lambda) - y_{sim}(\lambda; p)| \qquad (5)$$

with $y_{exp}(\lambda)$ the diffuse reflectance or autofluorescence intensity spectra acquired experimentally, $y_{sim}(\lambda; p)$ the diffuse reflectance or autofluorescence intensity spectra obtained from numerical simulation with $p = [\mu_a^A, \mu_a^M, \mu_a^I, \mu_s^A, \mu_s^M, \mu_s^I, g^A, g^M, g^I]^T$ the parameter vector to optimize. $Error(p)$ was minimized using a simplex optimization algorithm.

In order to quantify the difference between experimental and corresponding simulated spectra, we calculated the mean of normalized differences as follows:

$$Error_{mean} = \frac{1}{N} \sum_{i=1}^{N} \left| \frac{y_{exp}(\lambda_i) - y_{sim}(\lambda_i)}{y_{exp}(\lambda_i)} \right| \qquad (6)$$

III. RESULTS AND DISCUSSION

A. Mechanical results

The mean incremental elastic modulus curves shown in Fig. 3 are significantly different between fresh and cryopreserved vascular rings (p<0.05, Student T-test). We can notice that the mean incremental elastic modulus of post-cryopreserved samples is higher than the one of fresh samples. Other studies show similar significant differences in the behavior laws between fresh and post-cryopreserved arterial tissues [4].

However, some studies performed on arterial segments instead of rings founded values of circumferential stress and incremental elastic modulus to be higher for fresh arteries than for cyopreserved ones [29]. This apparent contradiction may be explained by the difference between these two types of tests (3D vs circumferential uniaxial). It has been observed that the values of stresses are higher, at identical strain, for tests on rings than for tests on arterial segments. Our results here obtained for the rings ($\sigma_{\theta\theta} = 0.15 \times 10^6$ N/m^2 for $\varepsilon_{\theta\theta} \approx 0.3$) are of the same order of magnitude when compared to other published ones [18].

A two-way ANalysis Of the VAriance (ANOVA) with repeated measures revealed that the values of incremental elastic modulus are significantly different between fresh and cryopreserved samples (all strains together), and between strains applied (whatever fresh or cryopreserved samples) since for this set of measurements, the values of F_{calc} (10.1, 38.7) were significantly superior to the critical values F_{crit} (3.9, 2.1), with a significance threshold of 5%. That is, deformations lead to significant differences in mechanical parameters measured, like cryopreservation does as well, but deformations and cryopreservation do not interact together ($F_{calc} = 0.1$, $F_{crit} = 2.1$). These results are listed in Table I.

B. Spectroscopic experimentation and simulation results

1) Autofluorescence results: Each autofluorescence intensity spectrum was normalized to its area under the curve between 470 and 810 nm. Figure 4(a) shows an example of such standardized spectra of fresh and cryopreserved samples obtained for a same deformation of $\varepsilon_{\theta\theta} = 30\%$. We may observe that the fresh sample curve has a higher amplitude than the cryopreserved sample one in the range 500-600 nm. Similar observation is made for all samples. Therefore, as shown in Fig. 4(a), we defined specific areas under the curve corresponding to sums of the intensities between 500 and 600 nm for fresh (A) and cryopreserved (C) spectra and between 600 and 810 nm respectively (B, D).

Then, autofluorescence spectrum area ratios $R_{fresh} = A/B$ and $R_{cryo} = C/D$ were calculated accordingly for each elongation leading to the graphs in Fig. 4(b). The variation of R_{fresh} and R_{cryo} as a function of circumferential strains $\varepsilon_{\theta\theta}$ tends to be linear with linear regression coefficients of 0.88 and 0.82 respectively for R_{fresh} and R_{cryo}.

A two-way ANOVA with repeated measures (see Table I) confirmed that the surface ratio values are significantly different ($F_{calc} >> F_{crit}$ with $p < 0.05$) between fresh and cryopreserved samples (all strains together), and between strains applied (whatever fresh or cryopreserved samples). That is, deformations lead to significant differences in autofluorescence signals measured, like cryopreservation does as well, but deformations and cryopreservation do not interact together ($F_{calc} = 0.3$, $F_{crit} = 2.1$). Thereby, whatever the strain, a fresh arterial ring can be differentiated from a post-cryopreserved one based on autofluorescence spectra measurements at 410 nm excitation and using wavelength band ratio calculation as proposed.

For fluorescence simulation, the optical properties of pure absorption and diffusion in the medium used at the excitation wavelength (410 nm) were extrapolated from the very few number of μ_a, μ_s and g values for intima, media and adventice found in the literature (values at $\lambda = 476, 580, 600, 633$ nm) [27] [28]. The following values were then implemented: $\mu_a(410) = 31/14/30$ cm^{-1} (A/M/I), $\mu_s(410) = 297/530/315$ cm^{-1} (A/M/I) and $g(410) = 0.71/0.89/0.79$ (A/M/I). The autofluorescence emission spectrum taken into account in our fluorescence simulation program was discretized from the spectral emission

TABLE I
TWO-WAY ANOVA STATISTICAL TEST PERFORMED WITH MECHANICAL DATA (INCREMENTAL ELASTIC MODULUS), AUTOFLUORESCENCE DATA
(SURFACE RATIO), AND DIFFUSE REFLECTANCE DATA FROM CHANNELS 1 AND 2.
INDEPENDANT VARIABLES (OR FACTORS) ARE THE FRESH/CRYOPRESERVED TYPES OF ARTERIES (2 LEVELS) AND THE STRAINS (7 LEVELS). ALL THE
GROUPS HAVE THE SAME SAMPLE SIZE ($n = 16$). F_{calc} AND F_{crit} ARE RESPECTIVELY THE CALCULATED AND CRITICAL VALUES OF THE F_{ratio}.

| | Mechanical data | | Autofluorescence data | | Diffuse reflectance data | | | |
| | | | | | Channel 1 | | Channel 2 | |
Sources of variations	F_{calc}	F_{crit}	F_{calc}	F_{crit}	F_{calc}	F_{crit}	F_{calc}	F_{crit}
Fresh / Cryopreserved	10.1 *	3.9	174 *	3.9	7.9 *	3.9	4.1 *	3.9
Strains	38.7 *	2.1	5.9 *	2.1	2.8 *	2.1	1.1	2.1
Interaction	0.1	2.1	0.3	2.1	0.2	2.1	0.5	2.1

* indicates that the difference between the data groups is statistically significant, for a significance threshold $p < 0.05$.

(a)　　　　　　　　　　　　　　(b)　　　　　　　　　　　　　　(c)
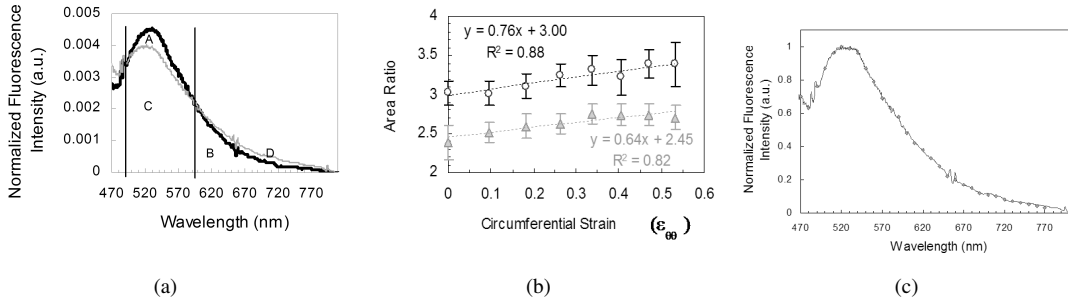
Fig. 4.   4(a) Example of autofluorescence intensity spectra normalized to the area under the curve (480-810 nm), for a 30% strain. The black and gray lines correspond respectively to the fresh and cryopreserved samples. A, B, C and D denote the areas under the spectral curves of the fresh artery rings between 500 and 600 nm (A) and between 600 and 810 nm (B), and of the cryopreserved ones between 500 and 600 nm (C) and between 600 and 810 nm (D). 4(b) Mean autofluorescence spectra area ratios for all the fresh samples A/B (black circles) and the cryopreserved ones C/D (gray triangles). 4(c) Example of experimental autofluorescence intensity spectra (full line) and corresponding simulated spectra (squares) of a fresh sample ($Error_{mean} = 3\%$).

curve previously measured on same artery samples under confocal microscopy and biphotonic excitation at 820 nm (see [11]). According to these measurements, the raised spectra of autofluorescence correspond mainly to the compound fluorescence of elastin and collagen networks in the media. Figure 4(c) shows the very good correlation between simulated and experimental spectra (mean normalized error less than 3%).

First, simulations were started with values of quantum yield and absorption coefficient for fluorescence μ_{af} (proportional to molar extinction and molecular concentration) adapted from the literature. We performed simulations at the 410 nm excitation wavelength with identical μ_{af} for all layers and searched for the values of μ_a, μ_s and g in the wavelength band of emission [470-770 nm] that give the best fit to the experimental curve of autofluorescence intensity for fresh arteries at 0% strain. Then, we varied μ_{af} in each layer (independently) in a wide range of values (typically [1-100] cm^{-1}) and as a result, we observed that the simulated autofluorescence intensity spectra vary in amplitude as a whole. Ratios given in Fig. 4 highlight the fact that these spectra (normalized spectra) are modified in shape when strains increase, with increasing amplitude in the lower wavelength band (500-600 nm) and decreasing amplitude in the higher one (600-810 nm). Varying μ_{af} allowed us to change the amplitude of the whole spectrum but not to deform it in such a way. Consequently, we decided to keep fixed values of μ_{af} and by optimization we found values of

the optical parameters (absorption, diffusion, anisotropy) of the medium in the wavelength band of emission allowing us to obtain proper shape variations of the autofluorescence spectra as a function of strains.

2) Diffuse reflectance results: Mean diffuse reflectance spectrum for fresh and cryopreserved artery rings are given in Fig.5(a).

Fig. 5(b) represents an example of measured and simulated diffuse reflectance spectra collected at inter-fibre distances of 0.53 mm (channel 1) and 1.74 mm (channel 2) and for three different strains applied to a cryopreserved sample. These results show spectra globally decreasing in light intensity as strain rises.

As indicated in Table I, a two-way ANOVA with repeated measures revealed that the values of ratio calculated from the channel 1 diffuse reflectance spectrum are significantly different ($p < 0.05$) between fresh and post-cryopreserved samples (all strains together), and between strains applied (whatever fresh or cryopreserved samples). For channel 2, these differences are much less or not significant indicating that, at the longest inter-fibre distance tested in our configuration, the diffuse reflectance ratio does not allow to differentiate between strains. This may be due to the low intensity level of the signal acquired. That is, deformations lead to significant differences in diffuse reflectance signals measured at the shortest inter-fibre distance (channel 1), like cryopreservation does as well, but deformations and cryopreservation do not interact together ($F_{calc} = 0.2$,

(a)   (b)
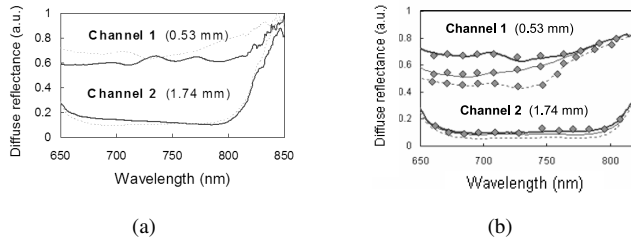
Fig. 5.   5(a) Mean diffuse reflectance spectrum acquired at 0% strain for fresh (full black line) and cryopreserved artery rings (gray dotted line), 5(b) Example of experimental diffuse reflectance spectrum (full line) and its corresponding simulated spectrum (points) for a cryopreserved sample, at two distances between emission and reception fibers (respectively 0.53 and 1.74 mm distances), at 3 different strains: 0% (full line), 30% (fine line) and 60% (dotted line).

$F_{crit} = 2.1$).

Both autofluorescence and elastic scattering spectroscopies gave intensity spectra with overall higher amplitude for the cryopreserved samples than for the fresh ones. It can correspond to either a decrease in light absorption and/or a more efficient light diffusion and fluorescence. These observation are to be related to the fact that cryopreservation affects the histological organization of the arterial wall (Fig. 2).

The spectral amplitude variations observed as a function of the level of deformation (increase of auto-fluorescence intensity and decrease of diffuse reflectance) can find an explanation in the fact that the samples in traction become increasingly thin as the deformation increases. The transmission of the light throughout the tissue thickness would be some thus increased, with the detriment of the back-scattered intensity collected. As the artery ring wall gets thinner under elongation, fluorescent compounds may potentially be excited with more energy, and the fluorescence emission intensity in the visible wavelength band (500-600 nm) reaching the surface may also be increased.

Finally, we observed significant variations in autofluorescence and diffuse reflectance spectra with reference to circumferential strains between 0% and 60%. Because these strains lead to structural reorganization of the arterial tissue and to decreasing of the artery wall volume probed by our fibered spectroscopic tools, it is of interest to investigate how the optical parameters of the tissue (μ_a, μ_s, and g) may consequently vary.

3) Optical parameters: In order to better understand the way optical properties differ between fresh and post-cryopreserved artery ring samples and between various levels of deformation, we calculated optimized values for the optical coefficients $\mu_a(\lambda)$, $\mu_s(\lambda)$ and $g(\lambda)$ in each of the three layers of the simulation model.

Bar graphs in Fig. 6 summarize the variations of absorption coefficient μ_a, scattering coefficient μ_s, and anisotropy factor g of the adventice (A), the media (M), and the intima (I), for fresh (F) and post-cryopreserved (C) samples with reference to three circumferential strains (0%, 26%, and 47%) and for three wavelengths: $\lambda = 700, 740, 780$ nm. From the mechanical tests, the mean values ($\pm$ SD) calculated for the wall thickness at 0, 0.26 and 0.47 strains were respectively of 0.5 (0.08), 0.19 (0.05), and 0.05 (0.006) mm for the fresh artery rings and of 0.69 (0.15), 0.34 (0.1), and 0.11 (0.03) mm for the post-cryopreserved artery rings.

Overall values of μ_a are found between 1 and 5.6 cm^{-1} while μ_s vary from about 130 (lower values for intima) up to 690 cm^{-1} (higher values for adventice) and g values from 0.8 up to 0.98.

At 700 and 740 nm, μ_a globally increases with the circumferential strain $\varepsilon_{\theta\theta}$. μ_a values of fresh samples are slightly higher than the ones of cryopreserved samples.

At 700, 740 and 780 nm, μ_s in adventice stay mainly at the same order of magnitude whatever $\varepsilon_{\theta\theta}$, while μ_s in media and intima vary more (decreasing with $\varepsilon_{\theta\theta}$ increasing). Values obtained for g are systematically higher in media and intima than in adventice. These results led to values of $\mu_{s'}$ between 41 and 131 cm^{-1} for the adventice, between 9 and 55 cm^{-1} for the media and between 1 and 79 cm^{-1} for the intima. Significantly higher values of $\mu_{s'}$ are found for the adventice compared to media and intima. They stay in the same order of magnitude whatever the type of sample (fresh or cryopreserved) and there is no clear tendency of their variations as a function of strains.

These results suggest that on average, the media and the adventice are respectively less and more absorbing for post-cryopreserved artery rings, regardless the wavelength, and it is the opposite for the fresh artery for $\lambda = 700, 740$ nm. Overall, we may notice that the values of absorption and diffusion coefficients are slightly higher for the fresh arteries than for the post-cryopreserved arteries, whatever the wavelengths and strains applied.

At our knowledge, there is up to now only few optical parameter values available from the literature for arterial tissues. [27] and [28] published the values of absorption, diffusion and anisotropy coefficient for adventice, media and intima layers of arteries for wavelengths of 476, 580, 600, 633 and 1024 nm. The optical parameter values found in the present study are in good agreement with their values at 633 nm ($\mu_a = 5.8/2.3/3.6$ cm^{-1}, $\mu_s = 195/310/171$ cm^{-1} and $g = 0.81/0.9/0.85$ for adventice/media/intima layers respectively) and at 1024 nm ($\mu_a = 2/1/2.3$ cm^{-1}, $\mu_s = 484/634/165$ cm^{-1} and $g = 0.97/0.96/0.97$ for adventice/media/intima layers respectively).

We observed on Fig. 5 that diffuse reflectance decreases with increasing strains which implies a globally lowered transport of light i.e. an increase of the optical coefficients combining absorption and diffusion (see Fig. 6), for both fresh and post-cryopreserved rings. The global stretch-induced increases in optical properties of tissue observed may be twofold. Firstly,

(a) $\lambda = 700$ nm

(b) $\lambda = 740$ nm

(c) $\lambda = 780$ nm
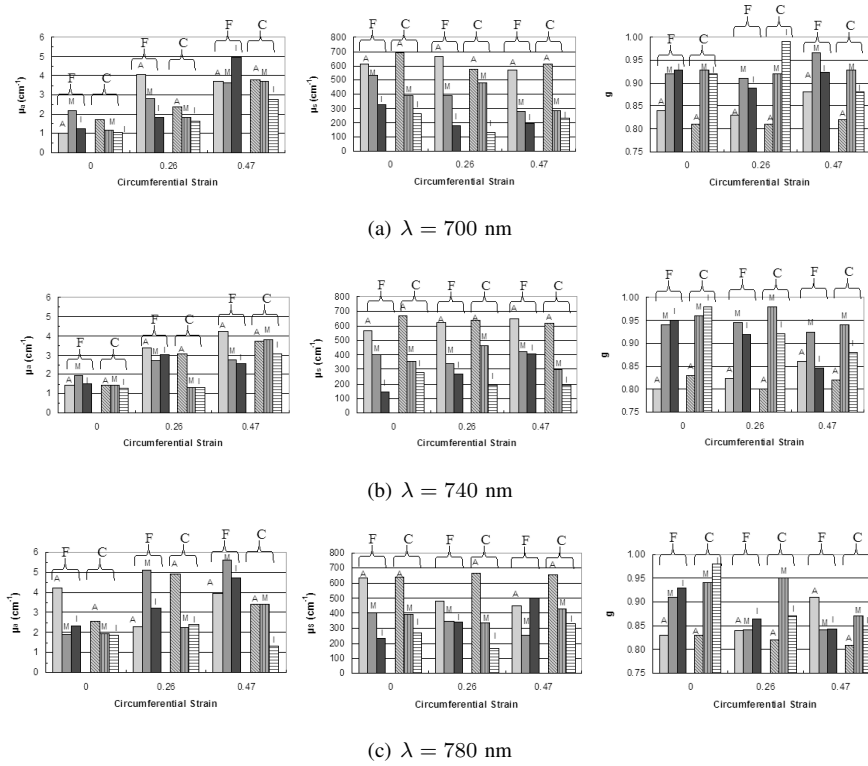
Fig. 6.   Values of absorption coefficient μ_a (left column), diffusion coefficient μ_s (center column) and anisotropy factor g (right column) for the adventice (A), the media (M), and the intima (I) with reference to three circumferential strains $\varepsilon_{\theta\theta}$ (0, 0.26 and 0.47) for fresh (F) and post-cryopreserved (C) samples, at three different wavelengths (top to bottom rows): 6(a) $\lambda = 700$ nm, 6(b) $\lambda = 740$ nm, 6(c) $\lambda = 780$ nm.

when the artery ring is stretched, the structural organization of the tissue changes (in particular the conformation of the extra-cellular matrix made of elastinic and collagenic fibers) as well as, for instance, the shape of the smooth muscular cells... Consequently, the intrinsic absorbing and diffusing properties of the medium are probably modified. This is also a consideration to have in the case of post-cryopreserved arteries to which structural alterations are associated. Furthermore, our results confirm that diffusion is dominant in arterial tissues (in agreement with other studies) and then, it contributes also significantly to the decrease of the back-scattered intensity measured. Secondly, it is also possible that the amount of light transmitted throughout the artery wall increases with the thickness decrease as strains rise leading to a decrease in the amount of back-scattered light which may also be interpreted as an increase in μ_a/μ_s. The only way to confirm that would be to measure the transmitted light which necessitates a more complex experimental configuration. Therefore, when the artery ring is stretched, it is quite difficult to relate the variations of the optical properties (absorption and diffusion) directly or only to chromophore densities (which would be the case if the medium would only change in volume but not in internal configuration) because these optical properties depend also on the anisotropic or inhomogeneous tissular "remodelling" process happening with the stretching.

In the case of arteries, common uniaxial traction tests on rings give rapid and simple access to a rheological characterization with limited instrumentation. In this configuration, the wall thickness variations of the ring under test can not be measured but is calculated with reference to the circumferential lengthening of the tissue. As confirmed in our study, the artery wall thickness is one the few parameters that influence the magnitudes of both fluorescence and diffuse reflectance signals. Therefore, other complementary spectroscopic studies should be performed on artery samples under mechanical constraints in configurations where the thickness can be experimentally measured.

IV. CONCLUSION

This study allowed us to obtain coupled results between rheological and optical (absorption, scattering, and fluorescence) properties of artery rings before and after cryopreservation, and at different levels of circumferential strains. We showed that the autofluorescence intensity spectra may be used to statistically differentiate between fresh and cryopreserved states of artery samples. Diffuse reflectance spectroscopy gave intensity spectra with overall higher amplitude for the cryopreserved samples than for the fresh ones. These observations are to be related to the histological modifications affecting the arterial wall of post-cryopreserved samples. We also observed significant spectral amplitude variations (increasing autofluorescence intensity and decreasing diffuse reflectance) as a function of the deformation applied to the artery wall (circumferential strains between 0% and 60%).

Using Monte Carlo simulation, we were able to identify values of absorption, diffusion and anisotropy coefficients and

their variations as a function of state (fresh and cryopreserved), strains (0, 30%, 60%) and wavelengths (700, 740, 780 nm). Overall, absorption and diffusion coefficients are slightly more important, whatever the wavelengths and strains applied, for the fresh artery than for the post-cryopreserved artery. Furthermore, the shape variations observed in the autofluorescence spectra due to strains were related to the modifications of the optical properties of the medium in the wavelength band of emission rather than to the changes in fluorescence absorption at excitation wavelength.

As implemented here, autofluorescence and diffuse reflectance spectroscopies may potentially be considered as simple complementary tools for tests of integrity or contactless characterization of the mechanical state of blood vessel tissues. Applications may concern for instance the pre- and per-operative evaluation of the mechanical compatibility between allograft and in situ arteries.

Finally, works are in progress to apply this approach to cutaneous tissues characterization with special interest in skin cancer diagnosis.

REFERENCES

[1] O. A'Amar and I. Bigio, "Spectroscopy for the Assessment of Melanomas," in *Reviews in Fluorescence 2006*, vol. 3. Springer, New York, 2006, pp. 359–386.

[2] I. Bigio and J. Mourant, "Ultraviolet and visible spectroscopies for tissue diagnostics: fluorescence spectroscopy and elastic-scattering spectroscopy," *Phys. Med. Biol.*, vol. 42, pp. 803–814, 1997.

[3] I. Georgakoudi, B. Jacobson, J. V. Dam, V. Backman, M. Wallace, M. Muller, Q. Zhang, K. Badizadegan, D. Sun, G. Thomas, L. Perelman, and M. Feld, "Fluorescence, reflectance, and light-scattering spectroscopy for evaluating patients with Barrett's Esophagus," *Gastroenterology*, vol. 120, pp. 1620–1629, 2001.

[4] W. Blondel, B. Lehalle, G. Maurice, X. Wang, and J. Stoltz, "Rheological properties of fresh and cryopreserved human arteries tested *in vitro*," *Rheol. Acta*, vol. 39, pp. 461–468, 2000.

[5] E. Rosset, A. Friggi, G. Novakovitch, P. Rolland, R. Rieu, J. Pellissier, P. Magnan, and A. Branchereau, "Effets de la cryoconservation sur les proprits viscolastiques des artres humaines," *Ann. Vasc. Surg.*, vol. 10, pp. 262–272, 1996.

[6] P. Dobrin, "Mechanical properties of arteries," *Physiol. Rev.*, vol. 58, no. 2, pp. 397–460, 1978.

[7] I. Cilesiz and A. Welch, "Optical properties of human aorta: are they affected by cryopreservation?" *Lasers Surg. Med.*, vol. 14, pp. 396–402, 1994.

[8] N. Ramanujam, *Encyclopedia of Analytical Chemistry*. Chichester: R.A. Meyers, 2000, ch. Fluorescence Spectroscopy In Vivo, pp. 20–56.

[9] G. Filippidis, G. Zacharakis, A. Katsamouris, A. Giannoukas, and T. Papazoglou, "Single and double wavelength excitation of laser-induced fluorescence of normal and atherosclerotic peripheral vascular tissue," *J. Photochem. Photobiol. B.*, vol. 56, pp. 163–171, 2000.

[10] M. Wallace, L. Perelman, V. Backman, J. Crawford, M. Fitzmaurice, M. Seiler, K. Badizadegan, S. Shields, I. Itzkan, R. Dasari, J. V. Dam, and M. Feld, "Endoscopic detection of dysplasia in patients with Barrett's esophagus using light-scattering spectroscopy," *Gastroenterology*, vol. 119, no. 3, pp. 677–682, 2000.

[11] C. Choserot, E. Pry, J. Goebel, D. Dumas, J. Didelon, J. Stoltz, and W. Blondel, "Experimental comparison between autofluorescence spectra of constrained fresh and cryopreserved arteries," *Clin. Hemorheol. Micro.*, vol. 33, pp. 235–242, 2005.

[12] E. Pry, W. Blondel, J. Goebel, J. Didelon, and F. Guillemin, "Spectral (optical) and mechanical responses of fresh and cryopreserved issued arteries," in *Proceedings of SPIE*, vol. 5695, 2005, pp. 66–74.

[13] T. Papaioannou, N. Preyer, Q. Fang, A. Brightwell, M. Carnohan, G. Cottone, R. Ross, L. Jones, and L. Marcu, "Effects of Fiber-Optic Probe Design and Probe-to-Target Distance on Diffuse Reflectance Measurements of Turbid Media: An Experimental and Computational Study at 337 nm," *Applied Optics*, vol. 43, no. 14, pp. 2846–2860, 2004.

[14] T. Pfefer, L. Matchette, and R. Drezek, "Influence of illumination-collection geometry on fluorescence spectroscopy in multilayer tissue," *Journal Medical and Biological Engineering and Computing*, vol. 42, no. 5, pp. 669–673, 2004.

[15] U. Utzinger and R. Richards-Kortum, "Fiber optic probes for biomedical optical spectroscopy," *Journal of Biomedical Optics*, vol. 8, no. 1, pp. 121–147, 2003.

[16] H. Demiray, "Large deformation analysis of some soft biological tissues," *J. Biomech. Eng.*, vol. 103, pp. 73–78, 1981.

[17] Y. Fung, *Biomechanics - Mechanical properties of living tissues*, 2nd ed. Springer-Verlag, 1993.

[18] R. Cox, "Comparison of arterial wall mechanics using ring and cylindrical segments," *Am. J. Physiol.*, vol. 244, pp. H298–H303, 1983.

[19] R. Shadwick, *Biomechanics, Structures and Systems: A Practical Approach*. A.A. Biewener, 1992, ch. Circulatory structure and mechanisms, pp. 233–261.

[20] A. Christy, S. Kasemsumran, Y. Du, and Y. Ozaki, "The detection and quantification of adulteration in olive oil by near-infrared spectroscopy and chemometrics," *Anal. Sci.*, vol. 20, no. 6, pp. 935–940, 2004.

[21] G. Viv-Truyols and P. Schoenmakers, "Automatic selection of optimal savitzky-golay smoothing," *Anal. Chem.*, vol. 78, no. 13, pp. 4598–4608, 2006.

[22] T. Tsai, H. Chen, C. Wang, J. Tsai, C. Chen, and C. Chiang, "*In vivo* autofluorescence spectroscopy of oral premalignant and malignant lesions: distorsion of fluorescence intensity by submucous fibrosis," *Lasers Surg. Med.*, vol. 33, pp. 40–47, 2003.

[23] Y. Louagie, "Viability of long-term cryopreserved human saphenous veins," *J. Cardiovasc. Surg.*, vol. 31, pp. 92–100, 1990.

[24] L. Wang, S. Jacques, and L. Zheng, "MCML - Monte Carlo modeling of light transport in multi-layered tissues," *Computer Methods and Programs in Biomedicine*, vol. 47, pp. 131–146, 1995.

[25] Q. Liu, C. Zhu, and N. Ramanujam, "Experimental validation of Monte Carlo modeling of fluorescence in tissues in the UV-visible spectrum," *Journal of Biomedical Optics*, vol. 8, no. 2, pp. 223–236, 2003.

[26] E. Pry, W. Blondel, C. Thomas, J. Didelon, and F. Guillemin, "Diffuse Reflectance Spectroscopy Monte-Carlo Modeling: elongated arterial tissues optical properties," in *IFAC Modelling and Control in Biomedical Systems (MCBMS'06)*, 2006, pp. 41–46.

[27] W. Cheong, S. Prahl, and A. Welch, "A review of the optical properties of biological tissues," *IEEE J. Quantum Elect.*, vol. 26, no. 12, pp. 2166–2185, 1990.

[28] G. Muller and A. Roggan, "Laser-Induced Interstitial Thermotherapy," P. of SPIE, Ed., vol. PM 25, Bellingham, WA, 1995.

[29] W. Blondel, J. Didelon, G. Maurice, X. Wang, and J. Stoltz, "Investigation of 3D Mechanical Properties Of Blood Vessels using A New In Vitro Tests System. Results On Sheep Common Carotid Arteries," *IEEE Trans. Biomed. Eng.*, vol. 48, pp. 442–451, 2001.